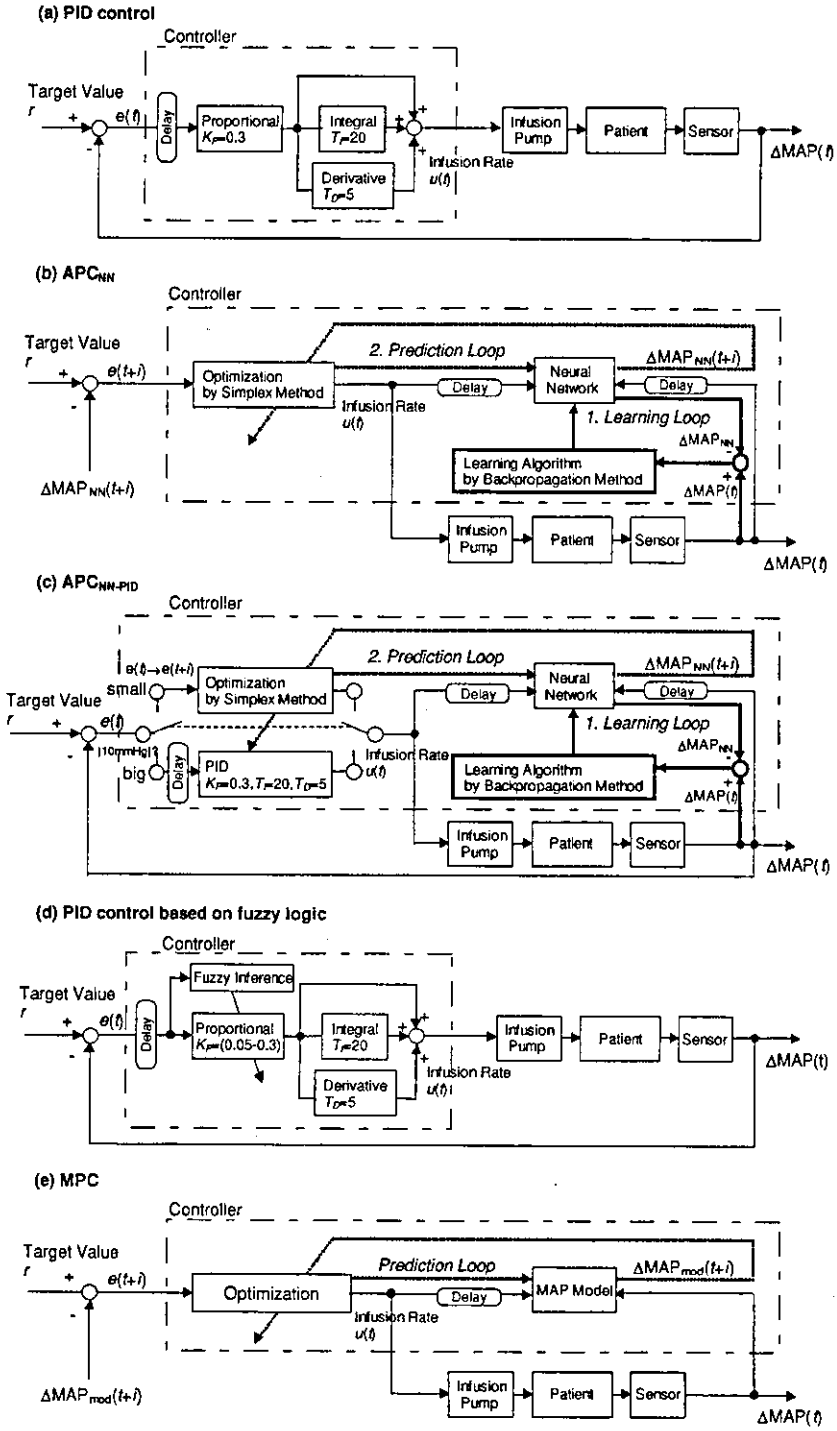

FIGURE 2. The block diagram for a MAP control system. (a) A proportional-integral-derivative (PID) control. (b) An adaptive predictive control using a neural network (APC_{NN}). (c) APC_{NN} combined with PID control ($APC_{NN\text{-}PID}$). (d) PID control based on fuzzy inference. (e) Model predictive control (MPC). $u(t)$: infusion rate of NE. r: a target value. $e(t)$: error between the target value and observed MAP. $e(t+i)$: error between the target value and MAP predicted by the NN ($\Delta MAP_{NN}(t+i)$) or the model MAP response ($\Delta MAP_{mod}(t+i)$). $\Delta MAP(t)$, ΔMAP_{NN}, and $\Delta MAP_{NN}(t+i)$ are actual changes in MAP, MAP changes by the NN before update, and changes in MAP predicted by the NN, respectively.

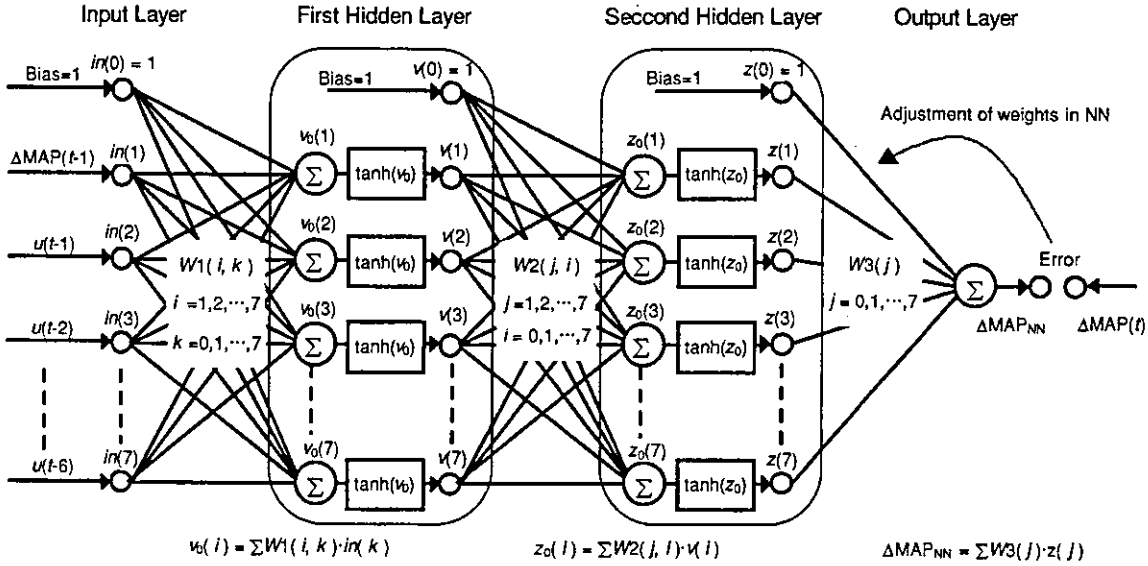

FIGURE 3. A four-layer feed-forward NN with two hidden layers to emulate the characteristics of a patient. The number of units in each hidden layer of the NN was set to seven (the same number as the input units). The NN had the unit bias. A hyperbolic tangent function [tanh(*x*)] was used as the output of each unit.

weights in the NN before the learning of the ΔMAP_{mod} response were assigned at random between -1 and 1. Then, the infusion rate of NE at $-4 \leq u(t) \leq 6$ $\mu g\ kg^{-1}min^{-1}$ was assigned at random and learning calls were replicated 50,000 times.[30] The ΔMAP_{mod} response during the learning process contained random noise between 0 and -5. Then, normalization was performed by dividing all outputs by 50 and the fixed learning rate was $K_n = 0.1$, which showed the most suitable number determined by a trial and error approach. This learning rate was smaller than that used for the actual MAP controls because it was necessary to avoid a local minimum.[25]

The absolute error between the ΔMAP_{mod} and the ΔMAP_{NN} response from the trained NN are shown in Fig. 1(c). Because of the random noise between 0 and -5, which emulated the hypotensive disturbances, the learning result of the NN showed an error of approximately 2 mmHg compared with the ΔMAP_{mod} data. The trained NN was used for the following simulation and animal studies, and the learning rate of the NN was set to $K_n = 0.2$ under the studies in order to quickly converge to the target value.[24,25,30]

As shown in Fig. 4(a), the goal of the APC_{NN} was to calculate the optimal NE infusion rate, $u(t)$, which minimized the following cost function $[J(t)]$,

$$J(t) = \sum_{i=1}^{N_p} [r(t+i) - \Delta MAP_{NN}(t+i)]^2 \qquad (7)$$

where N_p represents a prediction horizon, $r(t+i)$ is a prescribed target value of MAP control on time point $t+i$, and $\Delta MAP_{NN}(t+i)$ is the predicted MAP output by the NN. The future value of $\Delta MAP_{NN}(t+i)$ can be estimated by the $\Delta MAP_{NN}(t)$ acquired from the backpropagation algorithm [Fig. 4(a) and (b)]. $J(t)$ contained the predicted output after N_p steps to suppress sudden changes in NE infusion rate. The optimal value, $N_p = 3$, was obtained from a simulation using the ΔMAP_{mod}. A predicted response is also shown in Fig. 4(a) for $N_p = 3$. The cost function, $J(t)$, was minimized by a downhill Simplex method for a quadratic function (see Simplex Method for Quadratic Function under Appendix[16,30]).

Combined Control of APC_{NN} and PID ($APC_{NN\text{-}PID}$)

A NN can have many degrees of freedom to allow the learning of nonlinear time-varying characteristics of a patient, which, in turn, precludes the simultaneous optimization of stability and performance speed for the APC_{NN}.[1,14] Because emphasis is given to stability rather than speed in the algorithm's performance, the speed of MAP control was sacrificed to some extent. To supplement the speed performance, we constructed an APC_{NN} combined with a PID control. The PID algorithm in the $APC_{NN\text{-}PID}$ operates when the absolute error between observed MAP and a target value exceeds 10 mmHg [Fig. 2(c)]. Even when the PID control is operating, the NN continues learning the characteristics of a patient. The $APC_{NN\text{-}PID}$ used the same PID algorithm, NN learning rule, and cost function as those described in the Methods section under PID Control and Adaptive Predictive Control Based on a NN(APC_{NN}).

PID Control Based on Fuzzy Inference

Fuzzy inference[5] is the process of formulating and mapping from a given input to an output using fuzzy logic.[12,35] To adjust the proportional gain (K_P) of the PID controller

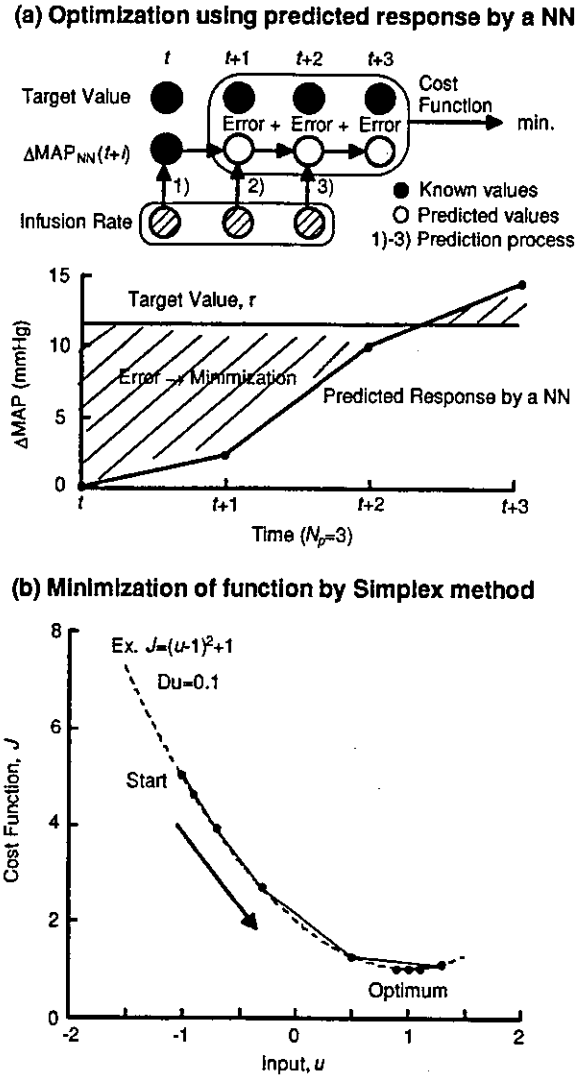

FIGURE 4. (a) Optimization of infusion rate using predicted response by a NN. (b) An example of minimization of a cost function by the downhill Simplex method for a quadratic function.

during the MAP control, a fuzzy inference system was used [Fig. 2(d)]. The basic structure for the adjustment of K_P is shown in Fig. 5. The inputs to the fuzzy inference system are the positive change from target value to $\Delta MAP(t)$ (overshoot, mmHg) and the difference between $\Delta MAP(t-1)$ and $\Delta MAP(t)$ (slope, mmHg 10 s^{-1}), and the output is the proportional gain, K_P, on the PID controller. The fuzzy inference process (Fig. 5) can be described as follows.

Step 1. Fuzzify Inputs. The first step is to take the inputs and determine the degree belonging to each of the appropriate fuzzy sets via membership functions (curves defining how each point in the input space is mapped to a degree of a membership function). In the present study, the triangular membership function formed by straight lines was used. The adjustment of K_P is built on three rules:

Rule 1. IF overshoot is small or slope is small THEN K_P is large.

Rule 2. IF overshoot is middle or slope is middle THEN K_P is middle.

Rule 3. IF overshoot is large or slope is large THEN K_P is small.

Each of the rules depends upon resolving the inputs into a number of different fuzzy linguistic sets: "overshoot is small," "slope is large," etc. The inputs must be fuzzified according to each of these linguistic sets. Step 1 in Fig. 5 shows how large the overshoot (rated on a scale of 5 to 15) or the slope (rated on a scale of 5 to 15) is via its membership functions [0, 1]. For example, when an overshoot of 8 (given our graphical definition of "overshoot is small") is selected, the degree of membership function corresponds to $\mu = 0.4$ for the "small" membership function. In this manner, each input is fuzzified over all the qualifying membership functions required by the rules.

Step 2. Apply Fuzzy Operator. The inputs to the fuzzy operator are two membership values from fuzzified input variables in Step 1, and the output is a single value. To determine the single output as the membership value, the OR operator was used in the present study[12]:

$$\mu_C = \max.\{\mu_A(x_1), \mu_B(x_2)\} \tag{8}$$

where $\mu_{(\cdot)}$ is the degree of the membership function. A and B are fuzzy sets in overshoot and slope and serve as inputs to the antecedent of the fuzzy rules. C is a fuzzy set in the values selected as the input to the consequent of the rules. The $x_{(\cdot)}$ is the input to the membership function. For example, when the antecedent of rule 1 is evaluated, two different pieces of the antecedent ("overshoot is small" and "slope is small") yield the fuzzy membership values 0.4 and 0, respectively. In this case, the OR operator selects the maximum of the two values, 0.4.

Step 3. Apply Implication Method. A consequent (K_P, a scale of 0.05–0.25) of the three rules is a fuzzy set represented by a membership function [0, 1] weighting appropriately the linguistic characteristics that are attributed to it. The consequent is reshaped using a function associated with the antecedent in order to determine a single number. The input for the implication process is a single number given by the antecedent, and the output is a fuzzy set. In the present study, an implication method was used by the AND operator[12]:

$$\mu_E(x_{3i}) = \min.\{\mu_C(x_{3i}), \mu_D(x_{3i})\} \quad i = 0, 1, \ldots, 20 \tag{9}$$

where C contains the values determined by Step 1. D is a fuzzy set in K_P for the antecedent of fuzzy rules. E is a fuzzy set in the values selected for the aggregation procedure (Step 4). The input range of $x_{(\cdot)}$ was divided by 20 to discretize the time domain. The AND operator selects the minimum of the two values as a single number given by the

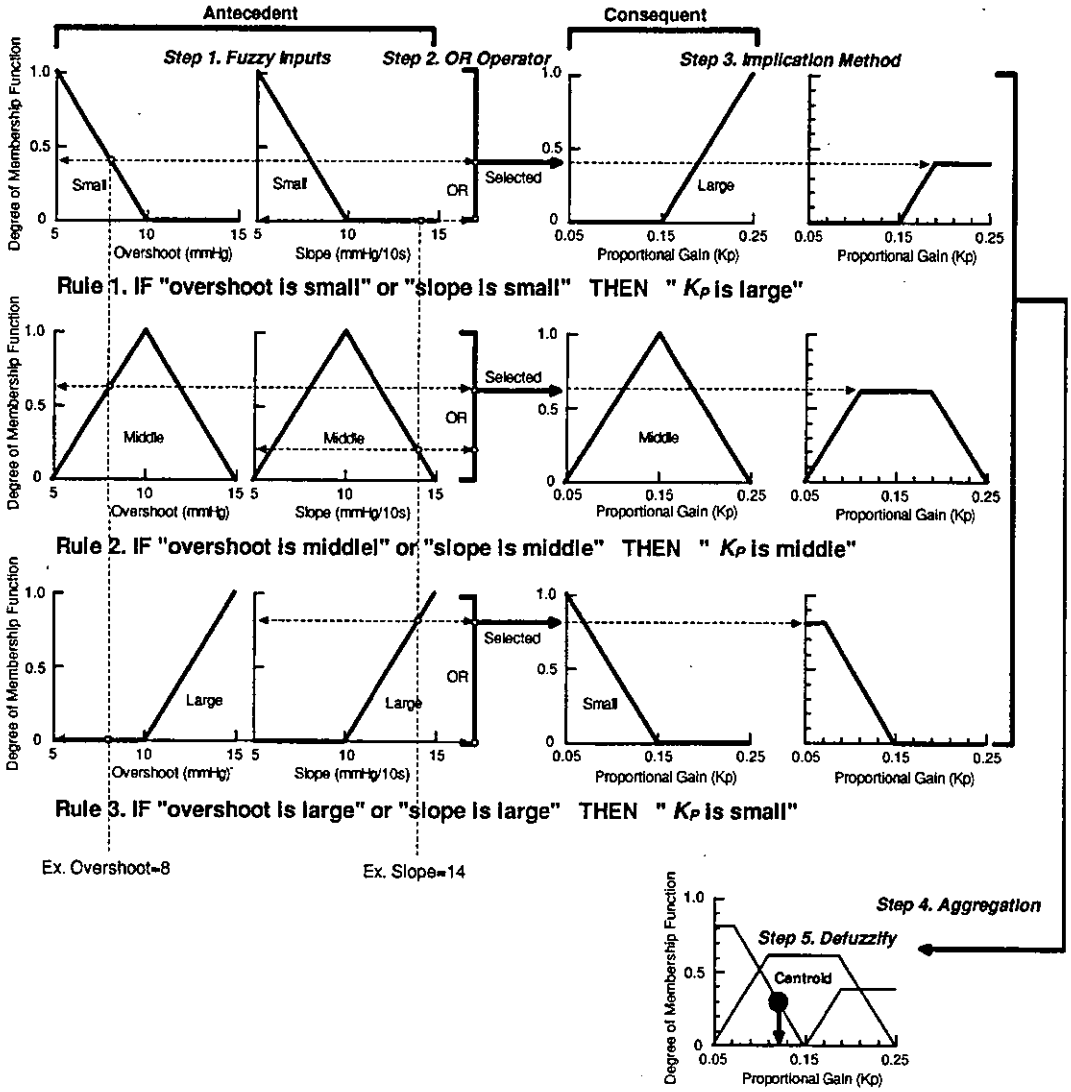

FIGURE 5. An example of a fuzzy inference system. The process for fuzzy inference is shown as Steps 1 to 5. The proportional gain (K_p) in the improved PID control was updated through the process for the fuzzy inference.

antecedent and the membership function of the consequent (Step 3 in Fig. 5).

Step 4. Aggregate All Outputs. Aggregation is the process by which the fuzzy sets that represent the outputs of each rule are combined into a single fuzzy set. Aggregation only occurs once for each output variable, just prior to the fifth and final step, defuzzification. The input of the aggregation process is the list of truncated output functions returned by the implication process for each rule. The output of the aggregation process is one fuzzy set for each output variable. The aggregation was performed by the selection of the maximum of two values in the membership functions[12]:

$$\mu_F(x_{3i}) = \max.\{\mu_{E1}(x_{3i}), \mu_{E2}(x_{3i}), \mu_{E3}(x_{3i})\}$$
$$i = 0, 1, \ldots, 20 \qquad (10)$$

where $E1$, $E2$, and $E3$ are the fuzzy sets determined by the Steps 1 to 4 under the rules 1, 2, and 3, respectively. F is a fuzzy set acquired from the result of the aggregation process. In Fig. 5, all three rules have been placed together to show how the output of each rule is combined, or aggregated, into a single fuzzy set whose membership function assigns a weighting for every output (K_P) value.

Step 5. Defuzzify. Because the aggregate of a fuzzy set encompasses a range of output values, it must be defuzzified in order to resolve a single output value from the set. The centroid calculation (center of gravity of the resulting curve) is used to determine the action that the controller will actually take. In the present study, the proportional gain for update, K_p^*, was calculated as follows[35]:

$$K_p^* = \frac{\sum_{i=0}^{20} \mu_F(x_{3i}) \cdot x_{3i}}{\sum_{i=1}^{20} \mu_F(x_{3i})} \qquad (11)$$

Model Predictive Control (MPC)

Figure 2(e) shows the diagram of the MPC. The drug infusion rate is computed to minimize the cost function [$P(t)$]:

$$P(t) = \sum_{i=1}^{N_p} [r(t+i) - \Delta\mathrm{MAP}_{\mathrm{mod}}(t+i)]^2 \qquad (12)$$

where N_p is a prediction horizon, $r(t+i)$ is a prescribed target value of MAP control on time point $t+i$, and $\Delta\mathrm{MAP}_{\mathrm{mod}}(t+i)$ is a model predicted output on time point $t+i$. $N_p = 3$ was used in the present study.

To calculate the future output, $\Delta\mathrm{MAP}_{\mathrm{mod}}(t+i)$, in the cost function, $P(t)$, we used the discrete linear step response model using the $\Delta\mathrm{MAP}_{\mathrm{mod}}(t)$ described in Methods under Modeling of MAP Response. The predicted output at the ith future point is shown as follows:

$$\Delta\mathrm{MAP}_{\mathrm{mod}}(t+i) = \sum_{\tau=0}^{i} g(\tau)\cdot\Delta T\cdot u(t+i-\tau) + \sum_{\tau=i+1}^{N_m} g(\tau)\cdot\Delta T\cdot u(t-\tau) + d(t) \qquad (13)$$

where $u(\cdot)$ is the infusion rate of NE (μg kg^{-1} min^{-1}) and $g(\cdot)$ is the unit impulse response (mmHg) which is consistent with that in Fig. 1(b). ΔT is the sampling interval (s) and N_m is the finite number of terms in the model of the unit impulse response. The parameters of $\Delta\mathrm{MAP}_{\mathrm{mod}}$ where $\Delta T = 10$ and $N_m = 30$ [Eq. (13)] includes 1) the present and all future moves of the manipulated variables that were used to solve the cost function, $P(t)$, 2) the past values of the manipulated variables (completely known at time t), and 3) the predicted disturbance calculated as the difference between the current measurements and output from the predicted model [$d(t) = \mathrm{MAP}_{\mathrm{mod}}(t) -$ actual MAP(t)] at the tth sampling time. The $d(t)$ represents model mismatch and unmodeled disturbances that enter the system at time t, and is assumed to be constant over the prediction horizon due to lack of an explicit means of predicting the mismatch or disturbance.[22]

Simulation Study

Protocol 1

We simulated MAP control using the $\Delta\mathrm{MAP}_{\mathrm{mod}}$ against acute hypotension. The exogenous pressure perturbation was introduced at a constant speed of -18 mmHg min^{-1} for 2 min, and then maintained at -36 mmHg for 5 min. Random noise within ± 1 mmHg was added to $\Delta\mathrm{MAP}_{\mathrm{mod}}$ and acute hypotension to mimic physiological variation. The target value of MAP control was set at the baseline MAP, i.e., $\Delta\mathrm{MAP} = 0$. The sampling interval was 10 s and each controller described below updated the NE infusion rate every 10 s. The NE infusion rate [$u(t)$) was bounded by $0 \le u(t) \le 6$ μg kg^{-1} min^{-1}]. The controllers used were the conventional PID controller, $\mathrm{APC_{NN}}$, and $\mathrm{APC_{NN\text{-}PID}}$. To see how the NN parameters changed as a function of time, the weights in the NN were recorded during $\mathrm{APC_{NN}}$ in the simulation study.

Protocol 2

To study the robustness to the MAP change to the drug, we simulated MAP control using the $\Delta\mathrm{MAP}_{\mathrm{mod}}$ [Fig. 1(b)], which was twice as large as the $\Delta\mathrm{MAP}_{\mathrm{mod}}$ response against acute hypotension. Because each controller was designed to optimize the controller performance under the assumption of the $\Delta\mathrm{MAP}_{\mathrm{mod}}$ response [Fig. 1(b)], the twice $\Delta\mathrm{MAP}_{\mathrm{mod}}$ response was unknown to all controllers. Random noise within ± 1 mmHg was added to $\Delta\mathrm{MAP}_{\mathrm{mod}}$. An exogenous pressure perturbation was introduced at a constant speed of -18 mmHg min^{-1} for 2 min, and then maintained at -36 mmHg for 5 min. The target value of MAP control was set at the baseline MAP. The sampling interval was 10 s and each controller updated the infusion rate of NE every 10 s. The infusion rate of NE [$u(t)$] was bounded by $0 \le u(t) \le 6$ μg kg^{-1} min^{-1}.

The controllers used were the conventional PID controller, $\mathrm{APC_{NN}}$, and $\mathrm{APC_{NN\text{-}PID}}$. In addition, to increase robustness during the MAP control, we tested PID control based on fuzzy inference for adjusting the proportional gain, K_P, during the closed-loop control. MPC was also tested in order to examine the performance of the simple predictive control compared with $\mathrm{APC_{NN}}$ or $\mathrm{APC_{NN\text{-}PID}}$.

Animal Study

The animal study conformed to the *Guide for the Care and Use of Laboratory Animals published by the US National Institutes of Health* (NIH Publication No. 85-23, revised 1996). The parameter values used in the simulation were also used in the animal study.

Surgical Preparations

Twelve Japanese white rabbits weighing 2.4–2.7 kg were anesthetized via intravenous injection (2 ml kg^{-1}) with a mixture of urethane (250 mg ml^{-1}) and α-chloralose (40 mg ml^{-1}). The rabbits were ventilated artificially with oxygen-enriched room air. To maintain the appropriate level of anesthesia, supplemental doses of the anesthetics were administered continuously (0.2–0.5 ml kg^{-1} h^{-1}, i.v.). MAP was measured using a high-fidelity pressure transducer (Millar Instruments, Houston, TX, USA) inserted into the right femoral artery. A catheter was introduced into the left femoral artery. A computer-controlled infusion pump (CFV-3200; Nihon Kohden, Tokyo, Japan) was attached to the arterial line for later arterial blood withdrawal and re-infusion. A double-lumen catheter was introduced into

the right femoral vein for administration of anesthetic agent and NE. Another computer-controlled infusion pump was used for NE infusion. The NE infusion rate was controlled through a 12-bit digital-to-analog converter connected to a laboratory computer. Body temperature was maintained at around 38°C with a heating pad throughout the experiment.

Protocols

To test the robustness of each control system, we used two different concentrations of NE. In Protocol 1 ($n = 6$), we used a NE solution of 25 μg ml^{-1}. In Protocol 2 ($n = 6$), which was performed in another group of rabbits, we used a NE solution of 50 μg ml^{-1}. In both Protocols 1 and 2, we first determined the volume of blood withdrawal necessary to induce a MAP fall of approximately 40 mmHg. The speed of blood withdrawal was calculated so that the hemorrhage was completed in 2 min. The average speed of blood withdrawal was 18.2 ± 6.8 ml min^{-1} in Protocol 1 and 20.2 ± 7.5 ml min^{-1} in Protocol 2.

In each hemorrhage trial, we recorded baseline MAP for 1 min prior to the hemorrhage and used the average baseline MAP as a target value. The arterial blood was then withdrawn at a predefined constant speed for 2 min to induce hemorrhage. Thereafter the hemorrhaged state was maintained for 5 min, rendering a total hemorrhage period of 7 min. We measured changes in MAP during hemorrhage under the uncontrolled condition, PID control, APC_{NN}, and $APC_{NN\text{-}PID}$. After 7 min of hemorrhage, the blood was slowly re-infused. We performed four trials (randomly ordered), in each rabbit, with a washout period of 20 min. Instantaneous MAP data was sampled continuously through a 12-bit analog-to-digital converter at 10 Hz and the MAP data (averaged every 10 s) was used as the system controlled variable.

Data Analysis

The performance of each controller was compared using several indices: maximum MAP fall during the initial 2 min of the hemorrhage (maximum fall), maximum absolute error between a target and observed MAP value calculated from the last 2 min of hemorrhage period (maximum error), and average absolute value of error between a target and observed MAP value over the entire hemorrhage period (average error). The elapsed time for MAP that first reached the target value within −5 mmHg (recovery time) was also calculated.

Statistical Analysis

All data were presented as mean ± SD. The differences of the performance indices among controllers were examined by one-way analysis of variance with repeated measures and the Bonferroni *post hoc* test.[7] Statistical significance was assigned to differences producing $p < 0.05$.

RESULTS

Simulation Study

Protocol 1

Figure 6 shows the simulation results from using (a) PID ($K_P = 0.3$, $T_I = 20$, and $T_D = 5$) control, (b) APC_{NN} ($K_n = 0.2$, and $N_p = 3$), and (c) $APC_{NN\text{-}PID}$ ($K_n = 0.2$, $N_p = 3$, $K_P = 0.3$, $T_I = 20$, and $T_D = 5$). Changes in MAP (left panels) and the NE infusion rate (right panels) are presented. The fall of MAP was −36 mmHg in 2 min and the hypotension continued for 5 min. In Fig. 6(a), (b), and (c), thick lines are MAP responses and thin lines are the uncontrolled condition. Dotted lines in Fig. 6(b) and (c) represent MAP responses predicted by the NN. When the controllers were activated, MAP returned to the target value. PID control with fixed parameters provided a quick and stable MAP regulation in the present simulation [Fig. 6(a), left]. APC_{NN} showed a maximum MAP fall greater than that of PID control [Fig. 6(b), left]. The recovery time was longer using APC_{NN} compared to PID control. The elevation in NE infusion rate was slow in APC_{NN} [Fig. 6(b), right]. $APC_{NN\text{-}PID}$ achieved MAP recovery faster than APC_{NN} [Fig. 6(c), left]. The PID component of the $APC_{NN\text{-}PID}$ system operated from 30 to 60 s when the MAP fall exceeded 10 mmHg.

Figure 7 shows the time series of the weights in the NN during the simulation study of APC_{NN} in the Protocol 1. Dotted lines in Fig. 7 represent the weights as bias. During the initial hypotension for 120 s, the weights as bias in the output layer [Fig. 7(c)] were dramatically decreased compared to the other weights, which were only slightly changed. Because the bias absorbed the offset of the acute hypotension, they would have kept the trained response characteristics to the infusion rate of NE in the NN. Therefore, it appears fine adjustments of the difference between the actual and NN-predicted MAP response were performed by modifications to the other weights in the NN.

Protocol 2

Figure 8 shows the simulation results of (a) PID ($K_P = 0.3$, $T_I = 20$, and $T_D = 5$) control, (b) APC_{NN} ($K_n = 0.2$ and $N_p = 3$), and (c) $APC_{NN\text{-}PID}$ ($K_n = 0.2$, $N_p = 3$, $K_P = 0.3$, $T_I = 20$, and $T_D = 5$) during the unexpected MAP change to NE, *i.e.* the magnitude of MAP change to NE was doubled. Changes in MAP (left panels) and the NE infusion rate (right panels) are presented. In Fig. 8(a), (b), and (c), thick lines are MAP responses and thin lines are the uncontrolled condition. Dotted lines in Fig. 8(b) and (c) represent MAP responses predicted by the NN. The fall of MAP was −36 mmHg in 2 min and

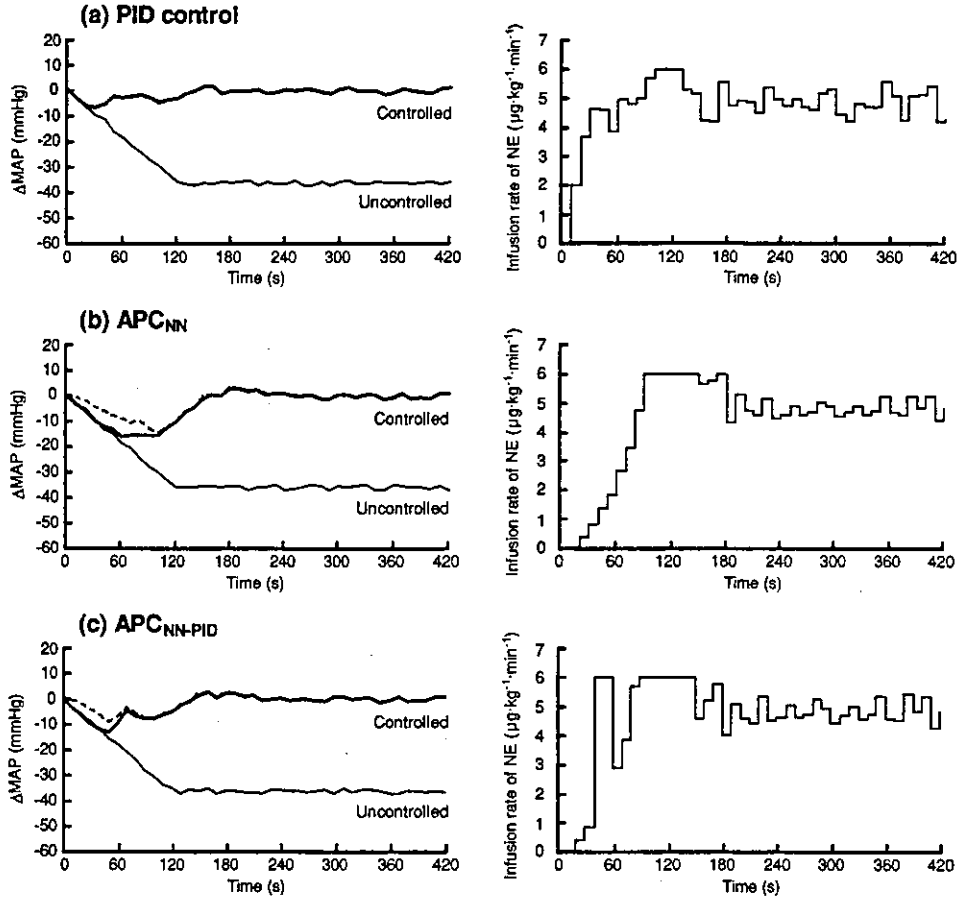

FIGURE 6. Simulation results of (a) PID control, (b) APC$_{NN}$, and (c) APC$_{NN-PID}$. The left panels show the MAP responses (thick solid line) and the uncontrolled condition (thin solid line). Dotted lines in (b) and (c) represent MAP responses predicted by the NN. The right panels show the NE infusion rate. Acute hypotension of −36 mmHg was completed in 2 min and maintained thereafter.

the hypotension continued for 5 min. Under PID control, although MAP returned to the target value within approximately 40 s, sustained MAP oscillation within ±10 mmHg occurred thereafter [Fig. 8(a), left]. The NE infusion rate cycled between 0 and the predefined maximum value. Under APC$_{NN}$, MAP decreased to −10 mmHg at 60 s, returned to the target value within approximately 120 s, exceeded the target value by approximately 10 mmHg at 150 s, and again returned to the target value at approximately 200 s [Fig. 8(b), left]. Under APC$_{NN-PID}$, MAP returned to the target value within approximately 70 s, exceeded the target value by approximately 10 mmHg at 100 s, and again returned to the target value at approximately 200 s [Fig. 8(c), left].

Figure 8(d) and (e) shows the simulation results of (d) improved PID control (initial parameters: $K_P = 0.3$, $T_I = 20$, and $T_D = 5$), and (e) MPC ($N_p = 3$) during the unexpected MAP change. Using improved PID control, MAP returned to the target value within approximately 60 s but had a slight oscillation within ±5mmHg (Fig. 8(d), left). The K_P was changed from 0.3 as the initial value to 0.187 at 40 s (slope > 5) and 0.193 at 50 s (actual ΔMAP > 5). Under MPC, although MAP returned to the target value within approximately 40 s, sustained MAP oscillation within ±10 mmHg occurred thereafter [Fig. 8(e), left]. The NE infusion rate cycled between 0 and 6 under the unexpected MAP change.

Animal Study

Protocol 1

Figure 9 shows typical examples of (a) PID ($K_P = 0.3$, $T_I = 20$, and $T_D = 5$) control, (b) APC$_{NN}$ ($K_n = 0.2$ and $N_p = 3$), and (c) APC$_{NN-PID}$ ($K_n = 0.2$, $N_p = 3$, $K_P = 0.3$, $T_I = 20$, and $T_D = 5$) obtained from one animal in Protocol 1. In Fig. 9(a), (b), and (c), thick lines are MAP responses and thin lines are the uncontrolled condition. Dotted lines in Fig. 9(b) and (c) represent MAP responses predicted by the NN. Under PID control, although MAP returned to the target value within approximately 60 s, four of six animals showed MAP oscillation within ±10 mmHg [Fig. 9(a), left]. Under APC$_{NN}$, MAP returned to the target value within approximately 120 s, exceeded the target value by approximately 5 mmHg at 150 s, and again returned

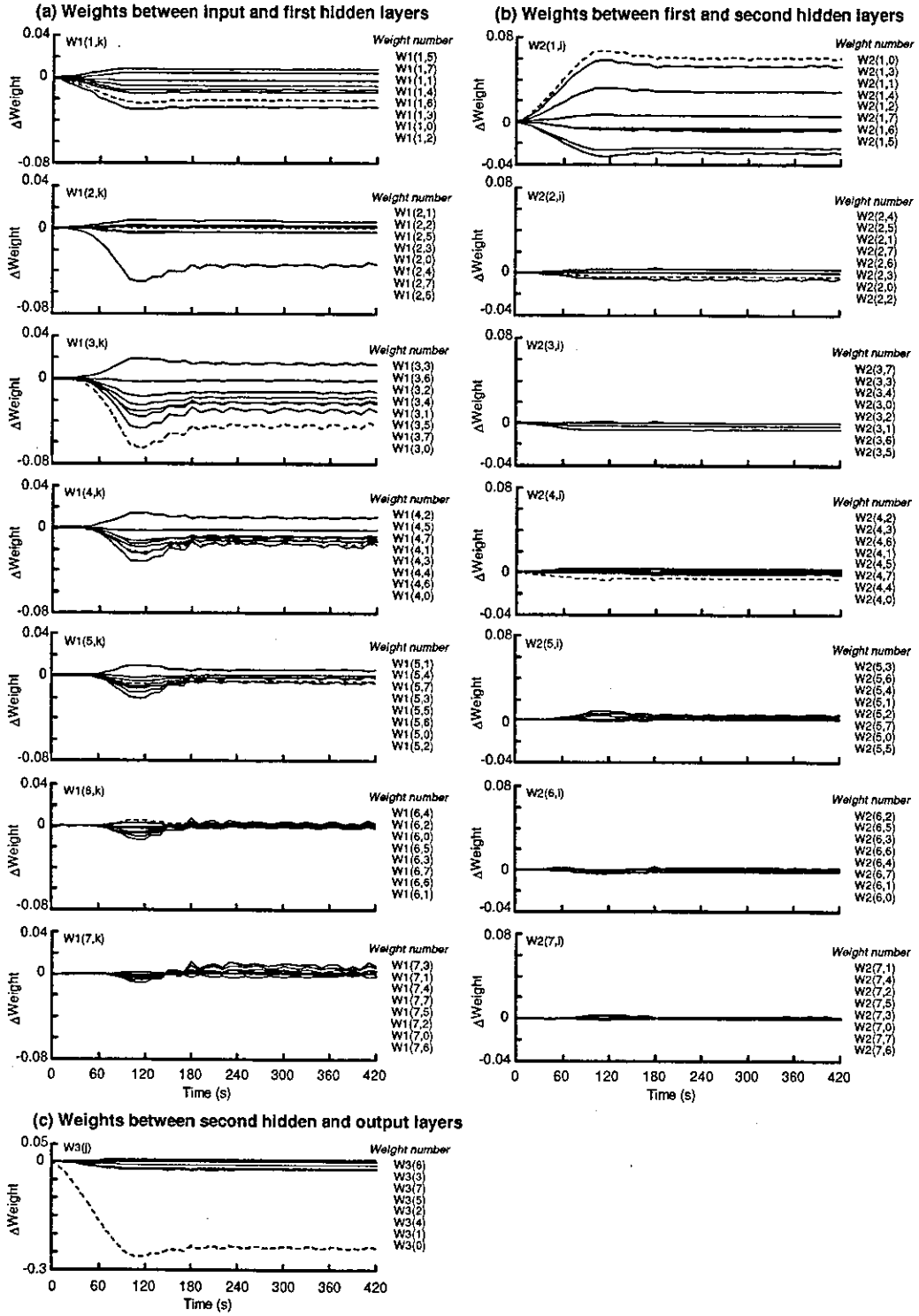

FIGURE 7. Time course of weight change from the weight at the starting time in the NN (Δweight) during the simulation study of APC_{NN} in Fig. 6 (b). (a) Weights between input and first hidden layers, (b) Weights between first and second hidden layers, and (c) Weights between second hidden and output layers. Weight numbers ($W1(i, k)$, $W2(j, i)$, and $W3(j)$) in the Figure correspond to those in Fig. 3. Each weight number was ordered from a high to low weight value at the final time. Dotted lines represent the weights as bias.

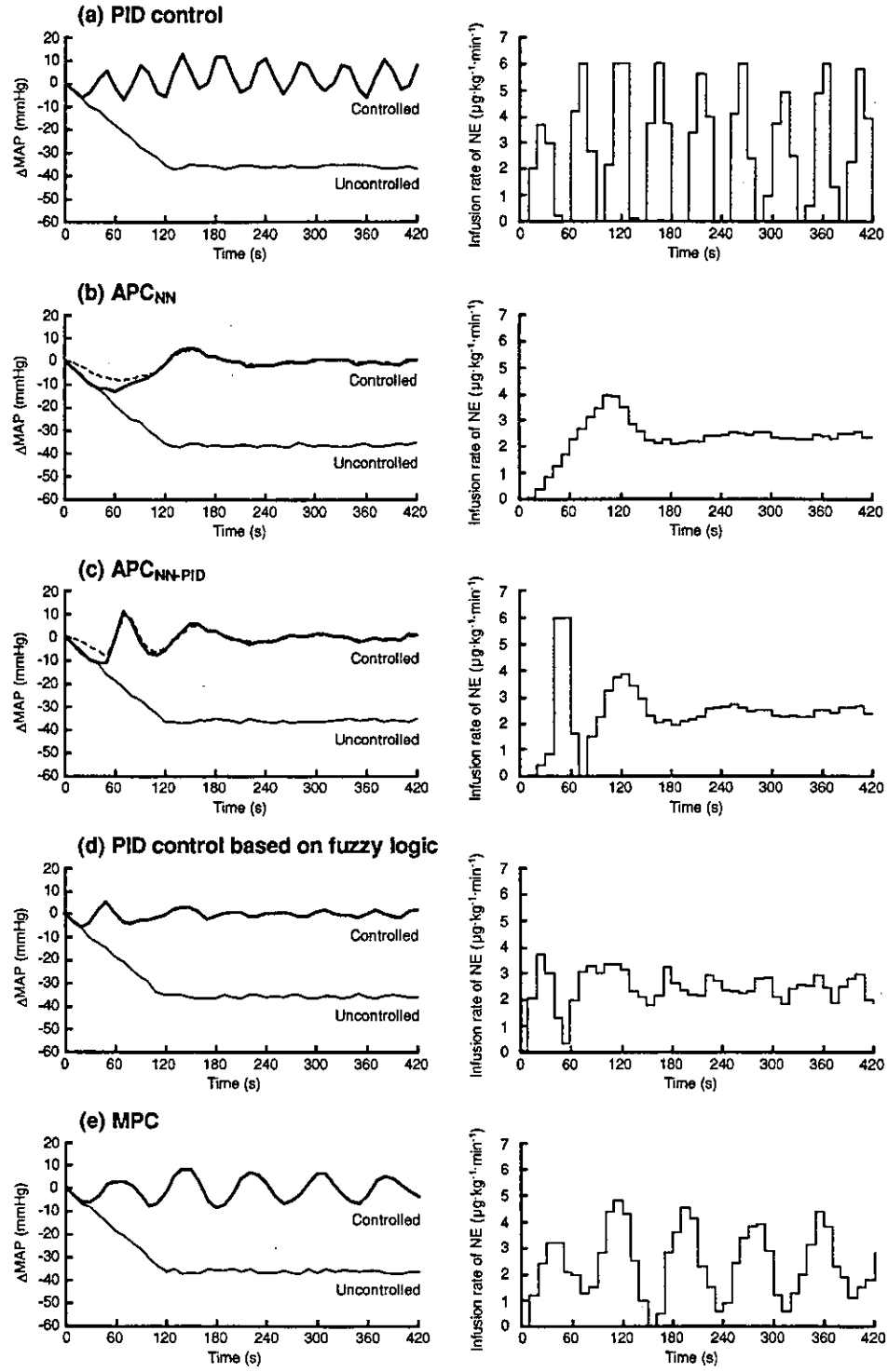

FIGURE 8. The simulation results of (a) PID control, (b) APC$_{NN}$, (c) APC$_{NN-PID}$, (d) PID control based on fuzzy inference, and (e) MPC under the unexpected MAP change. Left panels are changes in MAP and right panels are the NE infusion rate. Dotted lines in (b) and (c) represent MAP responses predicted by the NN.

to the target value at approximately 200 s [Fig. 9(b), left]. Under APC$_{NN-PID}$, MAP returned to the target value within approximately 60 s, exceeded the target value by approximately 8 mmHg at 150 s, and again returned to the target value at approximately 200 s [Fig. 9(c), left].

Figure 10 summarizes the performance indices obtained from Protocol 1. All controllers significantly attenuated the maximum MAP fall. The maximum MAP fall was greater in APC$_{NN}$ than in PID control. Neither maximum error nor average error differed among the three controllers. The

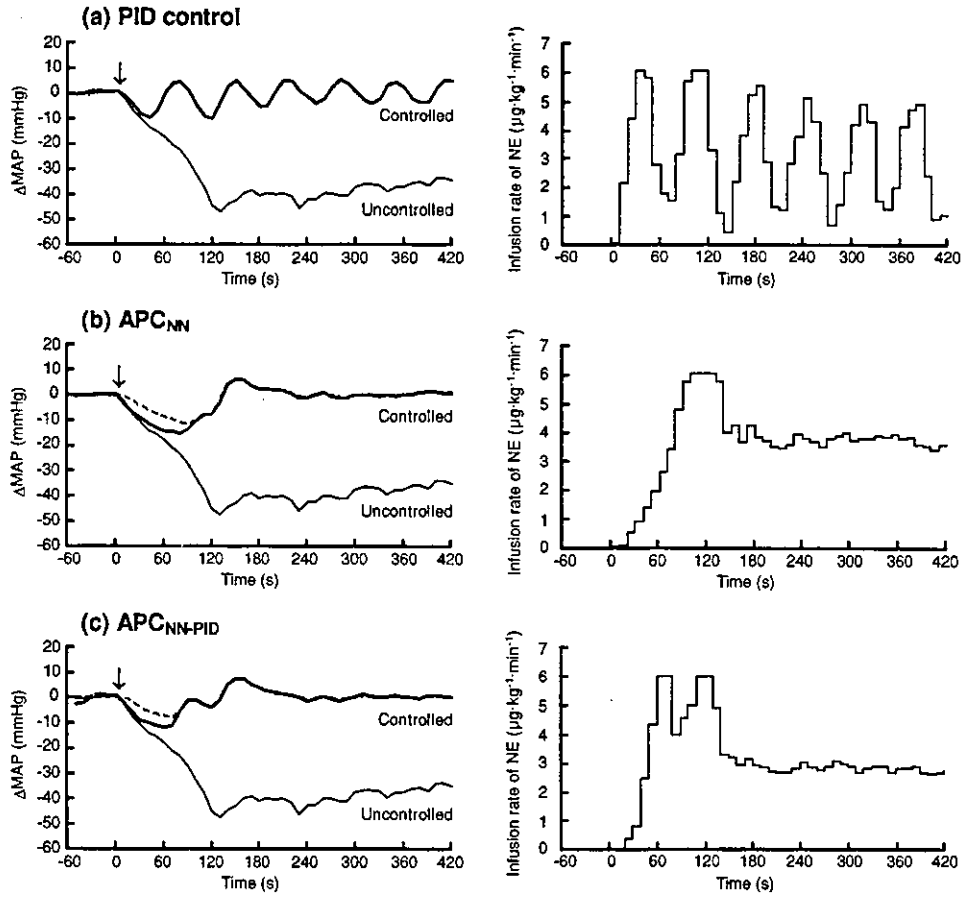

FIGURE 9. Typical examples of (a) PID control, (b) APC$_{NN}$, and (c) APC$_{NN-PID}$ obtained from one animal in Protocol 1. The left panels show the MAP responses (thick solid line) and the uncontrolled condition (thin solid line). Dotted lines in (b) and (c) represent MAP responses predicted by the NN. Arrows indicate the start point of hemorrhage and MAP control. The right panels show the NE infusion rate.

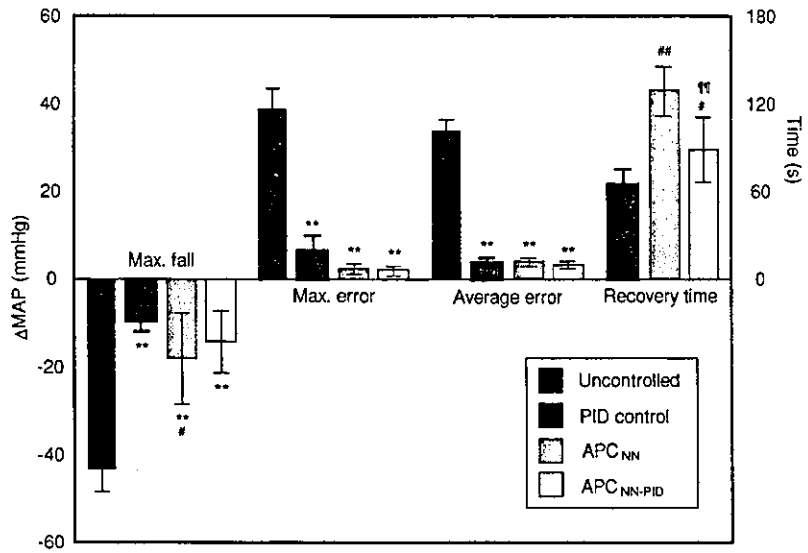

FIGURE 10. Maximum fall, maximum error, average absolute value of error between the target and observed MAP value (average error), and recovery time in the uncontrolled condition, PID control, APC$_{NN}$, and APC$_{NN-PID}$ obtained from Protocol 1. $^{**}P < 0.01$ vs. the uncontrolled condition. $^{\#\#}P < 0.01$ vs. PID control. $^{\#}P < 0.05$ vs. PID control. $^{\P\P}P < 0.01$ vs. APC$_{NN}$.

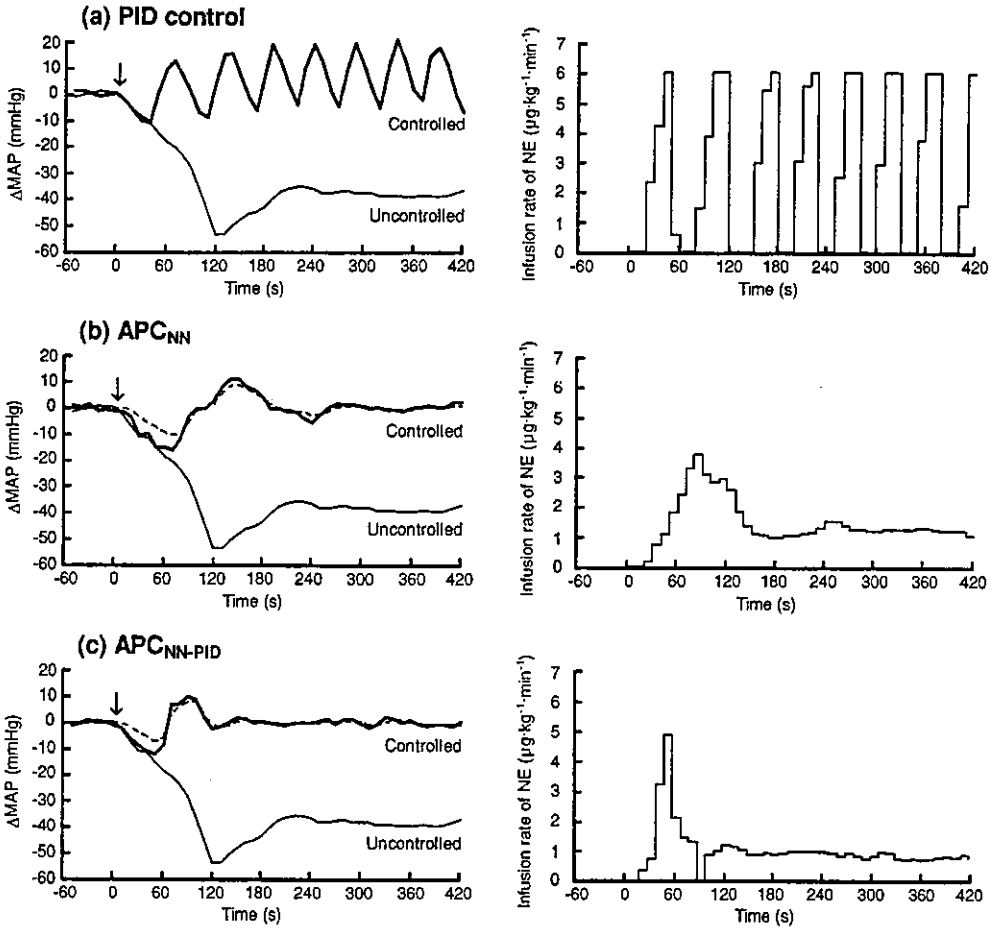

FIGURE 11. Typical examples of (a) PID control, (b) APC$_{NN}$, and (c) APC$_{NN-PID}$ obtained from one animal in Protocol 2. The left panels show the MAP responses (thick solid line) and the uncontrolled condition (thin solid line). Dotted lines in (b) and (c) represent MAP responses predicted by the NN. Arrows indicate the start point of hemorrhage and MAP control. The right panels show the NE infusion rate.

recovery time was significantly shorter in PID control than in APC$_{NN}$ and APC$_{NN-PID}$. The recovery time was significantly shorter in APC$_{NN-PID}$ than in APC$_{NN}$. The average blood loss was 14.1 ± 4.7 ml kg^{-1} body weight. The average MAP was decreased from 107.7 ± 9.1 to 73.9 ± 10.2 mmHg at 2 min of hemorrhage under the uncontrolled condition.

Protocol 2

Figure 11 shows typical examples of (a) PID (K_P = 0.3, T_I = 20, and T_D = 5) control, (b) APC$_{NN}$ (K_n = 0.2 and N_p = 3), and (c) APC$_{NN-PID}$ (K_n = 0.2, N_p = 3, K_P = 0.3, T_I = 20, and T_D = 5) in Protocol 2. In Fig. 11(a), (b), and (c), thick lines are MAP responses and thin lines are the uncontrolled condition. Dotted lines in Fig. 11(b) and (c) represent MAP responses predicted by the NN. Under PID control, although MAP returned to the target value within approximately 40 s, sustained MAP oscillation occurred thereafter in all six animals. In these animals MAP exceed the target value by 20 mmHg [Fig. 11(a), left]. The NE infusion rate cycled between 0 and the predefined maximum value. Under APC$_{NN}$, MAP returned to the target value within approximately 120 s, exceeded the target value by approximately 10 mmHg at 150 s, decreased by approximately 5 mmHg at 240 s, and again reached the target value at approximately 300 s [Fig. 11(b), left]. Under APC$_{NN-PID}$, MAP returned to the target value within approximately 70 s, exceeded the target value by approximately 10 mmHg at 100 s, and again reached the target value at approximately 120 s [Fig. 11(c), left].

Figure 12 summarizes the performance indices obtained from Protocol 2. All controllers significantly attenuated the maximum MAP fall. There were no significant differences in the maximum MAP fall among the three controllers. Both maximum error and average error were significantly smaller in APC$_{NN}$ and APC$_{NN-PID}$ than in PID control. The recovery time was significantly shorter in PID control than in APC$_{NN}$ and APC$_{NN-PID}$. The recovery time in APC$_{NN-PID}$ was significantly shorter than in APC$_{NN}$. The average blood loss was 15.5 ± 5.4 ml kg^{-1} body weight. The average

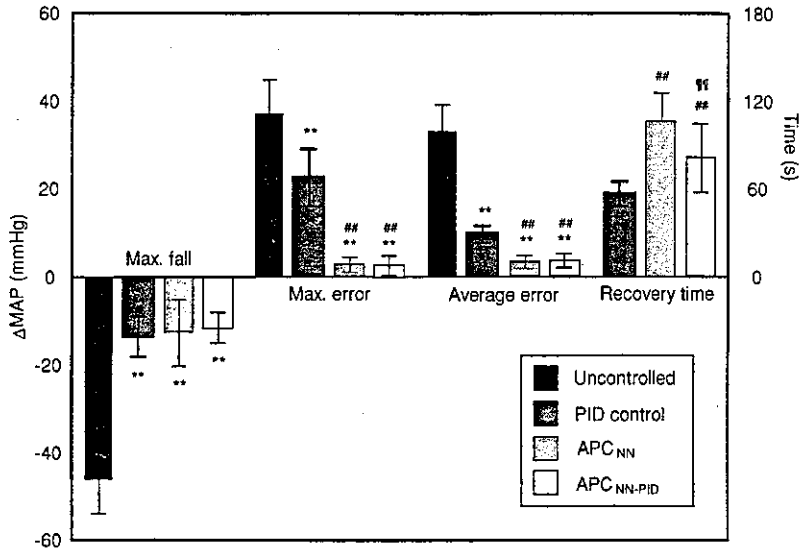

FIGURE 12. Maximum fall, maximum error, average error, and recovery time in the uncontrolled condition, PID control, APC_{NN}, and $APC_{NN\text{-}PID}$ obtained from Protocol 2. $^{**}P < 0.01$ vs. the uncontrolled condition. $^{\#\#}P < 0.01$ vs. PID control. $\P\P P < 0.01$ vs. APC_{NN}.

MAP decreased from 101.4 ± 9.9 to 68.4 ± 9.4 mmHg at 2 min of hemorrhage under the uncontrolled condition.

DISCUSSION

Prolonged hypotension below 45 mmHg could cause circulatory insufficiency in vital organs resulting in death.[8] The arterial baroreflex is an important negative feedback mechanism that maintains MAP at normal operating pressure against any pressure disturbance. In the present study, however, the average MAP fall exceeded −30 mmHg under the uncontrolled condition (Figs. 9 and 11). This is to say that the buffering effect of the arterial baroreflex was not sufficiently strong to prevent acute and severe hypotension despite the fact that the sympathetic system appears to have been maximally activated through the baroreflex negative feedback. All systems tested were able to prevent severe hypotension by controlling the infusion of NE, which acted on the heart, capacitance vessels, and resistance vessels to increase MAP. There might be a considerable reserve in the circulatory responses to NE even when the sympathetic system is fully activated through the baroreceptor unloading. Rapid action and the short half-life (approximately 2 min) of NE were convenient for MAP control using the automated drug infusion systems.

Although PID control did not show MAP oscillation in the simulation study [Fig. 6(a)], MAP oscillation within ±10 mmHg occurred in four of the six animals in Protocol 1 of the animal study [Fig. 9(a)]. Because PID parameters were tuned beforehand using a model of MAP response and fixed during the control periods, PID control could not optimize the MAP control with respect to individual animals. In Protocol 2 of the animal study, PID control failed to stabilize MAP in all animals [Fig. 11(a)]. A large MAP oscillation was sustained until the study was terminated at 7 min. These results suggest that using the PID control could endanger patients in clinical settings if the PID parameters are not individualized, which is unrealistic because the MAP response to NE infusion, in each subject, is unknown beforehand.

In the modeling of MAP response to NE, we used an average step response of 5 min during NE infusion in anesthetized rabbits without hemorrhage. If fine tuning of a PID controller is performed based on the pathological model of acute hypotension, the result of PID control in the animal study might have been better compared to the results from the present study. However, the modeling of MAP response to a therapeutic agent in acute hypotension is actually quite difficult due to the complex pharmacological variability and the various reactions to bleeding.

In contrast to PID control, the NN in APC_{NN} and $APC_{NN\text{-}PID}$ systems offer the ability to adapt to MAP changes based upon an individual's measurements, in real time, and learn the MAP response to NE infusion in respective animals. In Protocol 1 of the animal study, because hemorrhage itself was not predictable by the NN, ΔMAP predicted by the NN differed from measured ΔMAP in the initial phase of blood withdrawal [Fig. 9(b) and (c)]. However, ΔMAP predicted by the NN approximated the measured ΔMAP within 2 min, suggesting that the NN had learned the information required to control MAP. Thereafter, the MAP was stabilized at the target value in both APC_{NN} and $APC_{NN\text{-}PID}$. In Protocol 2 of the animal study, despite the use of a higher NE concentration, both APC_{NN} and $APC_{NN\text{-}PID}$ could prevent sustained MAP oscillation [Fig. 11(b) and (c)]. The maximum error and average error values in APC_{NN} and $APC_{NN\text{-}PID}$ were similar between Protocols 1 and 2 of the animal study, suggesting that the

control performance was not influenced by NE concentration. In other words, APC_{NN} and $APC_{NN\text{-}PID}$ might be able to adjust themselves for optimal MAP control even when the MAP response to NE infusion varied significantly among subjects.

Despite the potential benefit of automated drug infusion systems for MAP control, they have not been widely applied to routine clinical practice. One possible reason might be the difficulty in modeling the nonlinear MAP response to drug infusion.[9] Although various models of MAP response to drug infusion have been developed for MAP control,[22,34] the complexity of these models makes developing a reliable system controller difficult. In the present study, we used a simple first-order delay system as the model of MAP response to NE infusion. The initial connection weights for the NN were determined from the learning results of a linear model, yet APC_{NN} and $APC_{NN\text{-}PID}$ were able to maintain stable MAP regulation in the animal study. The flexibility of a NN coupled with an adaptive control mechanism enabled controlling the nonlinear system even if the controllers were initially designed using a linear model for the controlled system. Because utilization of a NN makes it unnecessary to construct a complex model for MAP response to drug infusion, it seems an ideal tool for designing a system to individualize MAP control in patients.

There are several limitations in the present study. First, to simplify the controller design we used a single control variable, i.e. the NE infusion rate. As the fluid infusion and blood transfusion as well as administration of other drugs are common in clinical practice, a multivariate control is mandatory for any reliable automated drug infusion system. Because a NN can have a multiple-input layer and multiple-output layer,[1] we will be able to extend APC_{NN} and $APC_{NN\text{-}PID}$ to multivariate control systems. Second, because we used a threshold value (± 10 mmHg) to activate PID control in $APC_{NN\text{-}PID}$, NE infusion rate changed discontinuously at $\Delta MAP = \pm 10$ mmHg. Although the discontinuity did not immediately cause the abrupt MAP change by virtue of the velocity form algorithm implemented for PID control, further refinement is required to suppress abrupt changes in the NE infusion rate.

The PID control based on fuzzy inference prevented the MAP response from having oscillations regardless of the unexpected MAP change [Fig. 8(d)]. We think the ideal result was due to the adaptive change of the proportional gain in the PID parameter. As a limitation, the PID controller based on the fuzzy inference has to be programmed with the known or experienced rules fit for the various cases in clinical settings. Because ascertaining all events under clinical circumstances is difficult, the design based on fuzzy rules may require an enormous setup stage. Under MPC, the MAP oscillation within ± 10 mmHg occurred under the unexpected MAP change [Fig. 8(e)] whereas MPC performed fine under the expected MAP change. In the case where the error between the MAP response in MPC and the actual MAP response is large, the cost function containing the weight of inputs or the model bank would be an effective way of adjusting the varying therapeutic sensitivities.[21] If the control conditions are within the expected ranges for the following disturbances; physiological sensitivities to therapeutic agents, interaction between agents, and variances of time dependent changes and nonlinearity; then the improved PID control, the MPC, and the conventional adaptive control will perform well. However, in the clinical setting, the control conditions are dynamic and unexpected patient response may occur. In this case, the model based predictive control or the fuzzy based control alone may not be able to adjust for the physiological changes. Therefore, adding the NN and fuzzy logic to the PID control, APC and MPC will be more effective for unexpected control conditions.

In conclusion, PID control, APC_{NN}, and $APC_{NN\text{-}PID}$ significantly prevented acute and severe hypotension induced by hemorrhage in anesthetized rabbits. Although PID control caused sustained MAP oscillation around the target value, the improved PID control based on fuzzy inference prevented the MAP from having this oscillation. Under the MPC, the MAP oscillation occurred under the unexpected control condition whereas the MPC performed ideally under expected control conditions. Designing a MPC or PID control based on fuzzy inference that is robust, may require an enormous amount of time to accurately model because of intra- and inter-patient variability in response to pharmacological drugs containing nonlinearity, pure time delay changes, and other unforeseen interactions and disturbances.[10,23] Both APC_{NN} and $APC_{NN\text{-}PID}$ showed more stable MAP control compared to PID control regardless of the NE concentration administered. The recovery time of $APC_{NN\text{-}PID}$ was shorter than that of APC_{NN}. Despite the simple design based on the first order delay model with unknown hypotension and drug sensitivity, the controls based on a NN approach were offered a robust control even in the presence of unexpected hypotension and unknown drug sensitivity. Therefore, utilization of a NN for adaptive predictive control would facilitate the development of an automated drug infusion system for quick and stable MAP control. However, further investigations using controls based on a NN will be required.

APPENDIX

Feed-Forward Output Using a NN

Input Layer to First Hidden Layer

The number of units in the first hidden layer of a NN was set to seven (the same number as the input units) using a trial and error approach. First, vector v_0 in the first hidden layer was calculated as follows:

$$v_0(i) = \sum_{k=0}^{7} W1(i,k) \cdot in(k) \quad i = 1, 2, \ldots, 7$$

where $W1(i, k)$ is the weight matrix, and $in(k)$ is the input to the first hidden layer. The inputs contain the unit bias, $in(0) = 1$.

The output of each neuron, $v_0(i)$, was transformed into $v(i)$ through a hyperbolic tangent function:

$$v(i) = \tanh\left(\frac{v_0(i)}{2}\right) = \frac{1 - \exp[-v_0(i)]}{1 + \exp[-v_0(i)]} \quad i = 1, 2, \ldots, 7$$

$v(0) = 1$ is the bias input to the second hidden layer.

First Hidden Layer to Second Hidden Layer

The number of units in the second hidden layer on a NN was set to seven (the same number as the first hidden layer units). $z_0(\cdot)$ was calculated as follows:

$$z_0(i) = \sum_{i=0}^{7} W2(j, i) \cdot v(i) \quad j = 1, 2, \ldots, 7$$

where $W2(j, i)$ is the weight matrix, and $v(i)$ is the input to the second hidden layer. The inputs contain the unit bias, $v(0) = 1$.

The output of each neuron, $z_0(j)$, was transformed into $z(j)$ through a hyperbolic tangent function:

$$z(j) = \tanh\left(\frac{z_0(j)}{2}\right) = \frac{1 - \exp[-z_0(j)]}{1 + \exp[-z_0(j)]} \quad j = 1, 2, \ldots, 7$$

$z(0) = 1$ is the bias input to the next output layer.

Second Hidden Layer to Output Layer

$\Delta\text{MAP}_{\text{NN}}$ in the output layer was calculated as follows:

$$\Delta\text{MAP}_{\text{NN}}(t) = \sum_{j=0}^{7} W3(j) \cdot z(j)$$

where $W3(j)$ is the weight matrix, and $z(j)$ is the input to the output layer. The inputs contain the unit bias, $z(0) = 1$.

Backpropagation Algorithm for Learning

The modification of weights in each layer on the NN can be described as follows.

Output Layer-Second Hidden Layer

$W3^*(j)$ is the weight matrix after update:

$$W3^*(j) = W3(j) - Kn \cdot \varepsilon \cdot \frac{\partial\text{MAP}_{\text{NN}}}{\partial W3(j)} \quad j = 0, 1, \ldots, 7$$

where

$$\frac{\partial\text{MAP}_{\text{NN}}}{\partial W3(j)} = z(j)$$

$z(j)$ is the input to output layer, which represents the output of each neuron in a hyperbolic tangent function on the second hidden layer.

Second Hidden Layer to First Hidden Layer

$W2^*(j, i)$ is the weight matrix after update:

$$W2^*(j, i) = W2(j, i) - Kn \cdot \varepsilon \cdot \frac{\partial\text{MAP}_{\text{NN}}}{\partial W2(j, i)}$$
$$j = 0, 1, \ldots, 7 : i = 0, 1, \ldots, 7 : v(0) = 1$$

where

$$\frac{\partial\text{MAP}_{\text{NN}}}{\partial W2(j, i)} = \frac{\partial\text{MAP}_{\text{NN}}}{\partial z(j)} \cdot \frac{\partial z(j)}{\partial z_0(j)} \cdot \frac{\partial z_0(j)}{\partial W2(j, i)}$$
$$= W3(j) \cdot \frac{1 - z(j)^2}{2} \cdot v(i)$$

$v(j)$ is the input to the second hidden layer, which represents the output of each neuron in a hyperbolic tangent function on the first hidden layer.

First Hidden Layer to Input Layer

$W1^*(i, k)$ is the weight matrix after update:

$$W1^*(i, k) = W1(i, k) - Kn \cdot \varepsilon \cdot \frac{\partial\text{MAP}_{\text{NN}}}{\partial W1(i, k)}$$
$$i = 1, 2, \ldots, 7 : k = 0, 1, \ldots, 7 : in(0) = 1$$

where

$$\frac{\partial\text{MAP}_{\text{NN}}}{\partial W1(i, k)} = \left[\sum_{j=1}^{7}\left(\frac{\partial\text{MAP}_{\text{NN}}}{\partial z(j)} \cdot \frac{\partial z(j)}{\partial z_0(j)} \cdot \frac{\partial z_0(j)}{\partial v(i)}\right)\right] \cdot \frac{\partial v(i)}{\partial v_0(i)} \cdot \frac{\partial v_0(i)}{\partial W1(i, k)}$$
$$= \left[\sum_{j=1}^{7}\left(W3(j) \cdot \frac{1 - z(j)^2}{2} \cdot w2(j, i)\right)\right] \cdot \frac{1 - v(i)^2}{2} \cdot in(k)$$

$in(k)$ is the input to the first hidden layer, which represents the past input to the NN.

Simplex Method for Quadratic Function

Figure 4(b) shows an example of the simplex method used to solve the quadratic function. The search starting at $u = -1$ reached the minimum point quickly. The steps of the downhill simplex method can be described as follows.[16,30]

Step 1. Calculate $Jx = J(Ux)$ of input Ux.
Calculate $Jy = J(Uy)$ of input $Uy = Ux + Du$ (initial change in quantity, ex. 0.1).

Step 2. Ja = the small number of Jx or Jy, and Ua = the input of the determined Ja.
The other output is Jb, and the input of Jb is Ub.
IF $Du < V$ (value showing convergence, ex. 0.001) THEN stop the Steps.

Step 3. $Uc = Ua + Du$ (opposite direction of Ub).
Calculate $Jc = J(Uc)$ in input Uc.
IF $Jc < Jb$ THEN go to Step 4, ELSE go to Step 5.

Step 4. $Ud = Uc + Du$ (opposite direction of Ub).
Calculate $Jd = J(Ud)$ of input Ud.
IF $Jd < Jc$ THEN $Du = 2 \cdot Du$, $Jx = Ja$, $Ux = Ua$, $Jy = Jd$, and $Uy = Ud$, ELSE $Jx = Jc$, $Ux = Uc$, $Jy = Ja$, and $Uy = Ua$.
Go to Step 1.

Step 5. Calculate $Du = Du/2$, $Ux = Ua$, $Jx = Ja$, $Uy = (Ua + Ub)/2$, and $Jy = J(Uy)$ of input Uy.
Go to Step 1.

ACKNOWLEDGMENTS

This study was supported by Research Grants for Cardiovascular Diseases (9C-1, 11C-3, 11C-7) from the Ministry of Health and Welfare of Japan, by a Health Sciences Research Grant for Advanced Medical Technology from the Ministry of Health and Welfare of Japan, by Grant-in-Aid for Scientific Research (B-11694337, C-11680862, C-11670730) and Grant-in-Aid for Encouragement of Young Scientists (13770378) from the Ministry of Education, Science, Sports, and Culture of Japan, by Research and Development for Applying Advanced Computational Science and Technology from the Japan Science and Technology Corporation, and by the Program for Promotion of Fundamental Studies in Health Science from the Organization for Pharmaceutical Safety and Research.

REFERENCES

[1]Chen, C. T., W. L. Lin, T. S. Kuo, and C. Y. Wang. Adaptive control of arterial blood pressure with a learning controller based on multilayer neural networks. *IEEE Trans. Biomed. Eng.* 44:601–609, 1997.

[2]Delapasse, J. S., K. Behbehani, K. Tsui, and K. W. Klein. Accommodation of time delay variations in automatic infusion of sodium nitroprusside. *IEEE Trans. Biomed. Eng.* 41:1083–1091, 1994.

[3]Fowler, N. O., and R. Franch. Mechanism of pressor response to l-norepinephrine during hemorrhagic shock. *Circ. Res.* 5:153–156, 1957.

[4]Franklin, G. F., J. D. Powell, and M. L. Workman. Digital Control of Dynamic Systems, 2nd ed. MA: Addison-Wesley, 1990, pp. 222–237.

[5]Fuzzy Logic Toolbox, User's Guide Manual, Version 2. Natick, MA: Mathworks, 2000.

[6]Gilmore, J. P., C. M. Smythe, and S. W. Handford. The effect of l-norepinephrine on cardiac output in the anesthetized dog during graded hemorrhage. *J. Clin. Invest.* 33:884–890, 1954.

[7]Glantz, S. A. Primer of Biostatistics, 4th ed. New York: McGraw Hill, 1997.

[8]Guyton, A. C. Textbook of Medical Physiology, 7th ed. Philadelphia: W. B. Saunders, 1986, pp. 326–335.

[9]Hoeksel, S. A., J. A. Blom, J. R. Jansen, J. G. Maessen, and J. J. Schreuder. Automated infusion of vasoactive and inotropic drugs to control arterial and pulmonary pressures during cardiac surgery. *Crit. Care Med.* 27:2792–2798, 1999.

[10]Huang, J. W., and R. J. Roy. Multiple-drug hemodynamic control using fuzzy decision theory. *IEEE Trans. Biomed. Eng.* 45:213–228, 1998.

[11]Isaka, S., and A. V. Sebald. Control strategies for arterial blood pressure regulation. *IEEE Trans. Biomed. Eng.* 40:353–363, 1993.

[12]Mamdani, E. H., and S. Assilian. An experiment in linguistic synthesis with a fuzzy logic controller. *Int. J. Man-Mach. Stud.* 7:1–13, 1975.

[13]Martin, J. F., A. M. Schneider, and N. T. Smith. Multiple-model adaptive control of blood pressure using sodium nitroprusside. *IEEE Trans. Biomed. Eng.* 34:603–611, 1987.

[14]Meline, L. J., D. R. Westenskow, N. L. Pace, and M. N. Bodily. Computer-controlled regulation of sodium nitroprusside infusion. *Anesth. Analg.* 64:38–42, 1985.

[15]Narendra, K. S., and K. Parthasarathy. Identification and control of dynamic systems using neural networks. *IEEE Trans. Neural Netw.* 1:4–27, 1990.

[16]Nelder, J. A., and R. Mead. A Simplex method for function minimization. *Comput. J.* 7:308–313, 1965.

[17]O'Hara, D. A., D. K. Bogen, and A. Noordergraaf. The use of computers for controlling the delivery of anesthesia. *Anesthesiology* 77:563–581, 1992.

[18]Pajunen, G. A., M. Steinmetz, and R. Shankar. Model reference adaptive control with constraints for postoperative blood pressure management. *IEEE Trans. Biomed. Eng.* 37:679–687, 1990.

[19]Quinn, M. L., N. T. Smith, J. E. Mandel, J. F. Martin, and A. M. Schneider. Automatic control of arterial pressure in the operating room: Safety during episodes of artifact and hypotension? *Anesthesiology* 68:A327, 1988.

[20]Rajfer, S. I., and L. I. Goldberg. Sympathomimetic amines. In: Principles and Practice of Acute Cardiac Care, edited by G. Das and S. Dipankar. Chicago: Year Book Medical, 1984, pp. 126–133.

[21]Rao, R. R., B. Aufderheide, and B. W. Bequette. Experimental studies on multiple-model predictive control for automated regulation of hemodynamic variables. *IEEE Trans. Biomed. Eng.* 50:277–288, 2003.

[22]Rao, R. R., B. W. Bequette, and R. J. Roy. Simultaneous regulation of hemodynamic and anesthetic states: A simulation study. *Ann. Biomed. Eng.* 28:71–84, 2000.

[23]Rao, R. R., J. W. Huang, B. W. Bequette, H. Kaufman, and R. J. Roy. Control of a nonsquare drug infusion system: A simulation study. *Biotechnol. Prog.* 15:556–564, 1999.

[24]Rumelhart, D. E., G. E. Hinton, and R. J. Williams. Learning representations by back-propagating errors. *Nature* 323:533–536, 1986.

[25]Rumelhart, D. E., G. E. Hinton, and R. J Williams. Learning internal representations by error propagation. In: Parallel Distributed Processing, Vol. 1, edited by J. L. McClelland, D. E. Rumelhart, and The PDP Research Group. Cambridge, MA: MIT Press, 1986.

[26]Schaer, G. L., M. P. Fink, and J. E. Parrillo. Norepinephrine alone versus norepinephrine plus low-dose dopamine: Enhanced renal blood flow with combination pressor therapy. *Crit. Care Med.* 13:492–496, 1985.

[27]Sheppard, L. C. Computer control of the infusion of vasoactive drugs. *Ann. Biomed. Eng.* 8:431–444, 1980.

[28]Stern, K. S., H. J. Chizeck, B. K. Walker, P. S. Krishnaprasad, P. J. Dauchot, and P. G. Katona. The self-tuning controller: Comparison with human performance in the control of arterial pressure. *Ann. Biomed. Eng.* 13:341–357, 1985.

[29]Sugimachi, M., T. Imaizumi, K. Sunagawa, Y. Hirooka, K. Todaka, A. Takeshita, and M. Nakamura. A new method to identify dynamic transduction properties of aortic baroreceptors. *Am. J. Physiol.* 258:H887–H895, 1990.

[30]Takahashi, Y. Adaptive predictive control of nonlinear time-varying system using neural network. *IEEE Int. Conf. Neural Netw.* 3:1464–1468, 1993.

[31]Tarazi, R. C. Sympathomimetic agents in the treatment of shock. *Ann. Intern. Med.* 81:364–371, 1974.

[32]Trajanoski, Z., and P. Wach. Neural predictive controller for insulin delivery using the subcutaneous route. *IEEE Trans. Biomed. Eng.* 45:1122–1134, 1998.

[33]Waller, J. L., and J. V. Roth. Computer-controlled regulation of sodium nitroprusside infusion in human subjects. *Anesthesiology* 63:A192, 1985

[34]Woodruff, E. A., J. F. Martin, and M. Omens. A model for the design and evaluation of algorithms for closed-loop cardiovascular therapy. *IEEE Trans. Biomed. Eng.* 44:694–705, 1997.

[35]Zadeh, L. A. Making computers think like people. *IEEE Spectr.* 8:26–32, 1984.

[36]Zieglar, J. G., and N. B. Nichols. Optimum settings for automatic controllers. *Trans. ASME* 64:759–768, 1942.

Faster oscillometric manometry does not sacrifice the accuracy of blood pressure determination

Masaru Sugimachi[a], Hirotsugu Okamoto[b], Sumio Hoka[b] and Kenji Sunagawa[a]

Faster oscillometry enables one to track rapid pressure changes. We therefore examined whether it was possible to shorten the measurement time without sacrificing accuracy. We accelerated and linearized cuff deflation and determined systolic and diastolic pressure values by the appearance and disappearance of oscillometric waves based on the interpolated cuff pressure-oscillometric wave amplitude relationship. The accuracy of faster oscillometry was examined by comparing correlations between invasive radial and oscillometric brachial pressure with either the conventional or the faster oscillometry in 23 patients (32 ± 16 measurement pairs). Faster oscillometry shortened the measurement time from 27.7 ± 3.5 s to 17.1 ± 2.6 s. Neither pressure levels nor heart rate altered the time required for measurement. Bland-Altman analysis indicated that mean and standard deviation of difference between oscillometric and invasive systolic pressure was comparable (conventional, 2.1 ± 7.5 mmHg; faster, 1.4 ± 7.3 mmHg) without correlations between difference and average of systolic pressure. Similar differences (conventional, 5.0 ± 6.8 mmHg; faster, 4.9 ± 5.8 mmHg) and lack of correlations were also found for diastolic pressure. In conclusion, we succeeded in shortening the oscillometric measurement time to approximately 60% of the original time without sacrificing accuracy. This was achieved by acceleration and linearization of cuff deflation and by interpolation of the relationship between cuff pressure and oscillometric wave amplitude. *Blood Press Monit* **9:135–141 © 2004 Lippincott Williams & Wilkins.**

Blood Pressure Monitoring 2004, 9:135–141

Keywords: measurement time, measurement error, accelerated linear deflation, algorithm with interpolation

[a]Department of Cardiovascular Dynamics, National Cardiovascular Centre Research Institute, Suita, Japan and [b]Department of Anesthesiology, Kitasato University Medical School, Sagamihara, Japan.

Correspondence and requests for reprints to Masaru Sugimachi, MD, PhD, Department of Cardiovascular Dynamics, National Cardiovascular Centre Research Institute, 5-7-1 Fujishirodai, Suita, Osaka 565-8565, Japan.
Tel: +81 6683 35012 ext. 2426; fax: +81 6683 55403;
e-mail: sugimach@ri.ncvc.go.jp

Received 5 December 2003 **Revised** 15 March 2004
Accepted 19 March 2004

Introduction

Blood pressure is one of the most important and ubiquitous variables for demonstrating the vital status of patients and its measurements are required almost everywhere in medical service. Although the invasive intra-arterial pressure measurements are taken as the gold standard due to its accuracy, introduction of non-invasive sphygmomanometric measurements dramatically widened the clinical use of blood pressure. In addition, the introduction of automatic oscillometric manometry greatly reduced the costs for human resources such as paramedical staff.

Despite its popularity, oscillometric manometry sometimes fails to meet the clinical requirements. One of the limitations is that this type of oscillometry is not intended to track rapid changes in pressure for example in operations and/or emergency rooms. Development of faster oscillometry ameliorates this limitation and improves the quality of medical services, especially in operating theatres, emergency rooms and intensive care units. Introduction of faster oscillometry is advantageous not only for such special medical services but also for regular wards and outpatient clinics. Faster oscillometry may enhance the merit of automatic manometry by saving measurement time, especially in the setting where many patients require measurement.

We therefore examined in this study whether faster oscillometry is feasible. We developed a faster oscillometry method by linearizing the deflation rate and by introducing a new pressure determination algorithm based on interpolated data from a small number of beats. We then determined the accuracy of this faster oscillometry and compared it with that of conventional oscillometry.

Patients and methods

Conventional oscillometric manometry

In conventional oscillometric manometry, the pulsatile components (oscillometric waves) can be detected in the gradually decreasing pressure measurements within a cuff that compresses the upper arm. Based on the relation between cuff pressure values and oscillometric wave amplitudes thus obtained, systolic, mean and diastolic pressure values are determined (Figure 1). Systolic pressure values are identified as the cuff pressure values at the rising edge of oscillometric wave amplitude, mean

1359-5237

DOI: 10.1097/01.mbp.0000130430.78823.42

Fig. 1

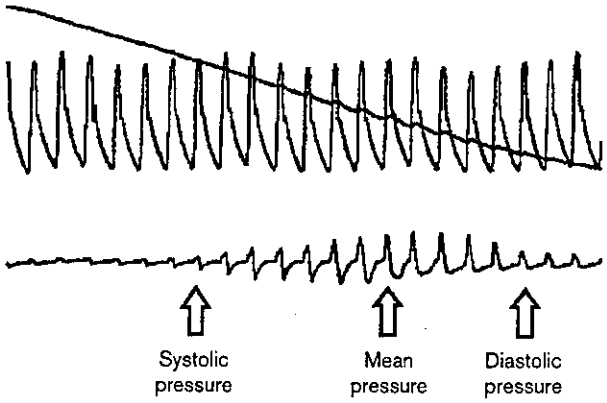

Cuff pressure tracing during oscillometric manometry from a patient, superimposed on simultaneously obtained invasive pressure tracing (top) and the oscillometric wave extracted from cuff pressure (bottom). The systolic, mean, and diastolic pressure values can be obtained from the cuff pressure values for oscillometric wave appearance, peak, and disappearance, respectively. Reproduced and modified with permission from Sugimachi M, Sunagawa K, Okamoto H, Hoka S. New algorithm for oscillometric non-invasive automatic arterial pressure measurement in patients with atrial fibrillation. *Masui* 2002; **51**:784–790.

pressure values as the cuff pressure values at its maximum amplitude, and diastolic pressure values as the cuff pressure values at the falling edge. The conventional oscillometric device is designed to determine these pressure values based on discrete cuff pressure values at each beat. Therefore, after identifying the beat at the rising edge, the beat for the maximal amplitude, and the beat at the falling edge the device determines the systolic, mean, and diastolic pressure values as the cuff pressure values at the corresponding beat. To warrant the number of beats for pressure determination analysis during each measurement, the conventional device is designed to adjust the deflating rate in the late deflation phase.

New faster oscillometric manometry

Besides the acceleration of cuff deflation (from 4–7 mmHg/s [conventional oscillometry at initial deflation] to 11–13 mmHg/s [our faster oscillometry]), to create faster oscillometry, we modified a conventional oscillometric device (BX-10, Colin Corporation, Komaki, Japan) by first, fixing the deflation rate but did not try to adjust the deflating rate to warrant the number of beats. We used a constant deflation rate because, in our preliminary study, changes in cuff deflation rates seem to distort the relationship between cuff pressure and oscillometric wave amplitude. Second, to compensate for the decrease in the number of beats, we interpolated the cuff pressure-oscillometric wave amplitude relationship between the discrete data obtained for each beat. Using the interpolated relationship, we determined the exact cuff pressure values at the time of the appearance of the oscillometric wave, its peak, and subsequent disappearance, rather than choosing cuff pressure values from several beats. We then adopted these cuff pressure values for oscillometric systolic, mean, and diastolic pressure values.

Data collection

To compare the accuracy of the faster oscillometric method with the conventional one, we conducted a clinical study using 36 patients who underwent scheduled surgery at Kitasato University Hospital and required invasive blood pressure monitoring for clinical reasons. There were 16 male and 20 female patients, and they were 56.1 ± 16.2 (16–82) years old. Of these 36 patients, three were excluded from the study for frequent arrhythmias, one for prominent pressure fluctuations synchronous to ventilation, and four for technical reasons that prohibited accurate invasive manometry.

In reference to Figure 2, a 20-gauge intra-arterial catheter was inserted into the radial artery of patients to monitor invasive arterial pressure. We used a commercially available manometer system (MP5200 [TW], Nihon-Kohden, Tokyo, Japan) for invasive pressure with the frequency response (100 Hz) sufficient for the determination of systolic and diastolic pressure values. This pressure served as the gold standard. In order to monitor blood pressure non-invasively simultaneously using the oscillometric method, a cuff was attached around the

Fig. 2

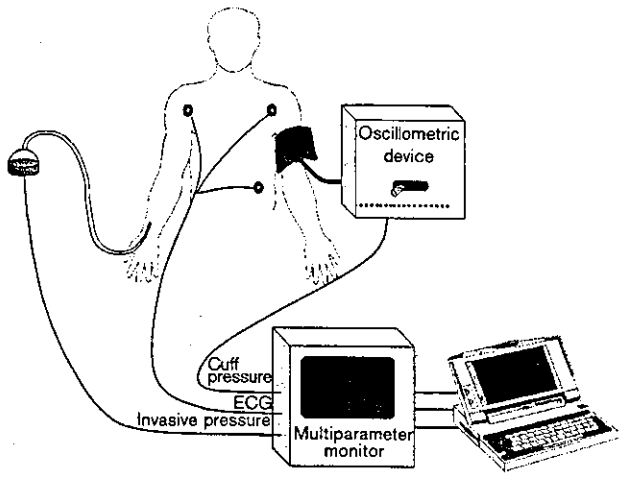

Illustration of an experimental set-up. Blood pressure was measured by a modified oscillometric device every 5 min, with simultaneous invasive pressure recording at the contralateral radial artery. The oscillometric device was switched alternately between the conventional and the faster deflation mode. Signals of invasive pressure, electrocardiogram, and cuff pressure with superimposed oscillometric wave were transferred to a multiparameter monitor and converted to a digital form for the offline analysis.

contralateral upper arm. Oscillometric measurements were performed at 5-min intervals. The cuff was connected to the custom oscillometric device modified for the above requirements based on the conventional oscillometric device (BX-10, Colin Corporation, Komaki, Japan). The device was switched alternately between the conventional and the faster deflation mode every 5 min so that both conventional and faster oscillometry were performed every 10 min.

Although we did not measure blood pressure with the conventional and the faster oscillometry at the same time, we measured invasive arterial pressure throughout all the oscillometric measurements so that one could compare the invasive and non-invasive pressure values. All satisfactory measurements during the surgery were used for analysis. Throughout the operation, signals of electrocardiography, invasive blood pressure, and cuff pressure (with imposed oscillometric wave) were transmitted to a multiparameter monitor (Model 86S, Agilent Technologies, Palo Alto, California, USA), converted to digital signals (1 kHz, 12 bits) (DAQ-CARD-700, National Instruments Corp., Austin, Texas, USA) and stored on a hard disk of a dedicated laboratory computer (Latitude HX500T, Dell Inc., Round Rock, Texas, USA) for the offline analysis. We did not use the electrocardiographic signal to determine blood pressure values.

Data analysis

In each patient, we compared invasive systolic and diastolic pressure values with those obtained by conventional oscillometry, and with those obtained using the faster oscillometry technique, using different pressure readings (average of 28 ± 17 readings) occurring throughout the operation. At this time, a further five patients with < 10 pressure readings were excluded from the analysis. This resulted in 23 patients (32 ± 16 pressure readings, range: 10–68 readings) for final analysis. Both systolic (87 ± 18 mmHg to 145 ± 17 mmHg, range: 75 ± 20 mmHg) and diastolic pressure (48 ± 9 mmHg to 79 ± 9 mmHg, range: 31 ± 10 mmHg) changed considerably during the operation.

Using these comparisons, we quantified the accuracy of the pressure values by the mean and standard deviation of the difference between the invasive and oscillometric pressure values. Invasive pressure values were obtained from the raw pressure signals stored on the hard disk, and all systolic and diastolic pressure values were averaged, respectively, during the corresponding oscillometric manometry.

To identify the possible influence of pressure levels (systolic, diastolic, and pulse pressure) and heart rate on the measurement time and the accuracy of the faster oscillometric technique, we investigated the correlations between these variables.

Statistical analysis

Data were expressed as mean ± standard deviation. Correlations between variables were obtained by linear regression analysis. Coefficients of determination (r^2) were reported.

Results

Figure 3 shows the comparison between measurement time with conventional oscillometry (open bars) and that with the faster oscillometry (solid bars). As expected the faster oscillometry shortened the time needed for pressure measurement to 62% that of the original (conventional, 27.7 ± 3.5 s; faster, 17.1 ± 2.6 s). We examined whether pressure level (one of systolic, diastolic, pulse pressure values) or heart rate serves as an obstacle to shorten pressure measurements. Figure 4 described the relation between one of these factors and measurement time of the faster oscillometric technique. Poor correlations between these factors and measurement time (systolic pressure, $r^2 = 0.08$; diastolic pressure, $r^2 = 0.04$; pulse pressure, $r^2 = 0.07$; heart rate, $r^2 = 0.02$) indicated that none of these factors served as hindrance factors to shorten pressure measurements.

In Figure 5 we compared systolic (left panel) and diastolic (right panel) pressure distribution obtained from pooled measurements by conventional (open bars)

Fig. 3

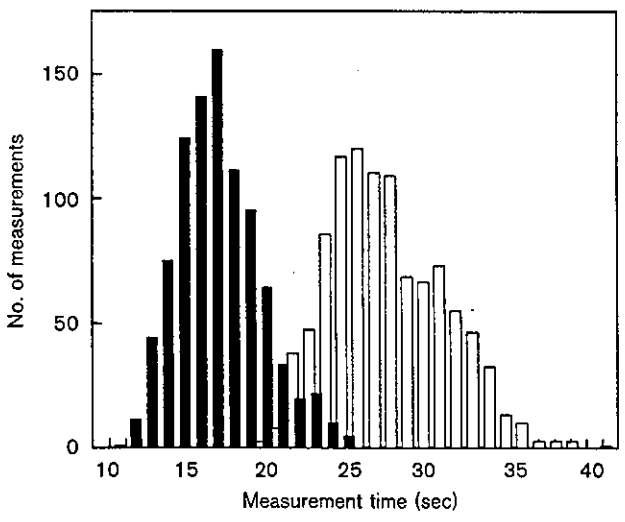

Comparison between pressure measurement time of conventional oscillometry (open bars) and that of the faster oscillometric method (solid bars). Measurement time was tabulated into 1 s bins and shown by a histogram.

Fig. 4

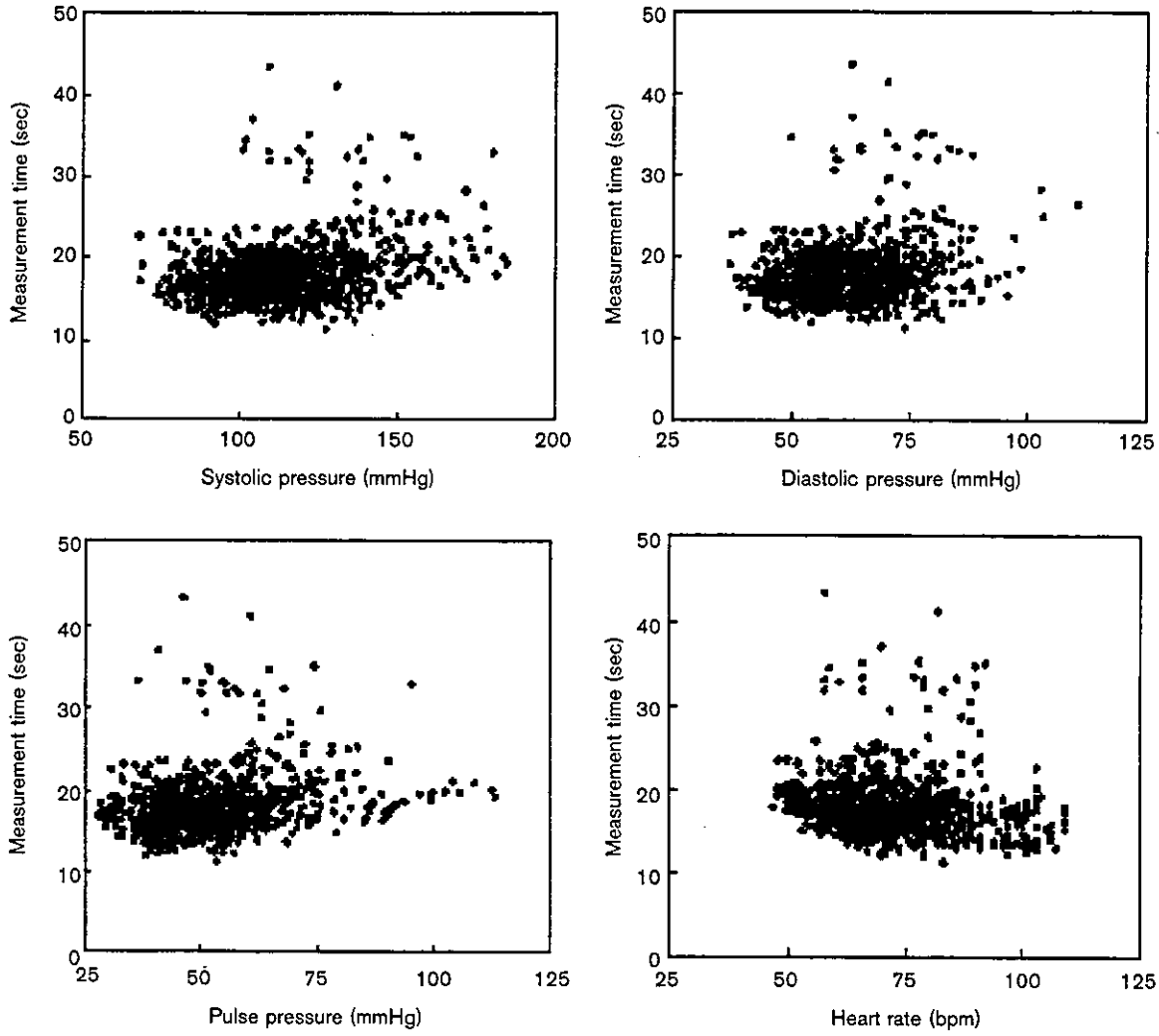

Effects of pressure values (systolic, diastolic and pulse pressure), and heart rate on pressure measurement time were examined by scattergrams. Invasive pressure values were used for independent variables.

and faster (solid bars) oscillometry. These histograms show the similarity of pressure values obtained by the two different oscillometric methods as a whole, though the corresponding two measurements were 5 min apart.

Figure 6 illustrates the accuracy of the conventional (bottom panels) and the faster (top panels) oscillometry by plotting measurement error (oscillometric minus invasive pressure) against the average invasive and oscillometric pressure (Bland-Altman method) [1–2]. The left panels show Bland-Altman plots for systolic pressure measurements. The limit of agreement (mean ± SD of the error, dashed and dotted lines) was comparable between the conventional (2.1 ± 7.5 mmHg) and the faster oscillometry (1.4 ± 7.3 mmHg). Correlation between the error and systolic pressure level was weak (r^2 = 0.08). The right panels show Bland-Altman plots for diastolic pressure measurements. The limit of agreement (dashed and dotted lines) was also comparable between the conventional (5.0 ± 6.8 mmHg) and the faster oscillometry (4.9 ± 5.8 mmHg), and correlation between the error and diastolic pressure level was also weak (r^2 = 0.04).

In Figure 7, we examined possible influences of other pressure levels (average of invasive and oscillometric pressure) or heart rate on measurement error of systolic and diastolic pressure, respectively, determined by the faster oscillometric method. Poor correlations were found between measurement errors for systolic pressure and